Optimizing Actuation of Assembly of DNA Origami Nano Structures

Jingyuan Wang

Undergraduate Thesis, Spring 2021

Bachelor of Science in Mechanical Engineering

The Ohio State University

Department of Mechanical and Aerospace Engineering

Nanoengineering and Biodesign Laboratory

Thesis Defense Committee:

Dr. Carlos Castro, Department of Mechanical and Aerospace Engineering (Advisor)

Dr. Ratnasingham Sooryakumar, Department of Physics

Co-Mentor:

Dr. Anjelica Kucinic, Department of Chemical Engineering

Abstract

DNA origami as an advanced nanotechnology has been useful in providing precise design and construction for nanostructures. Combining with different actuation mechanisms such as toehold mediated strand displacement (TMSD) or magnetic actuation can realize precise control in planar or spatial motion for nanoscale structures. Recent efforts have expanded DNA origami to micrometer scale nanostructures by integrating many nanocomponents into larger assemblies, and a key goal of this work is to achieve real-time multiplexing actuation over these micron-scale assemblies. Firstly, focusing on a stiff micro-scale DNA lever assembly, this work has tested different assay conditions including varying concentrations, incubation time and purification parameters to optimize the yield of individual DNA origami structure sub-units as a basis for higher order lever assembly. Also this work aims to maximize yield of at least 1-2 micrometer polymerized nanostructures, which represents a key step for practical multiplexing. Secondly, moving towards assemblies with complex reconfiguration capabilities, a verification of reconfigurability and complex motion for a second structure system was conducted. The second system consists of a DNA origami structure comprised of 6-bars connected into a closed loop. The structure can be reconfigured into several different shapes including a rectangle, triangle, hexagon, and flat closed shape. Broadly speaking, this work has integrated optimized construction for a magnetic actuated nanopolymer and verification of the feasibility of reconfiguration for a nanostructure with high order degree of freedoms. This work expands the possibilities for complex design and practical construction at micrometer scale which enables real-time control over DNA origami structures with complex reconfiguration.

Acknowledgement

I would like to appreciate the instruction and patience from my advisor Dr. Carlos Castro and my mentor Anjelica Kucinic! Also I appreciate the help from all the members in Nanoengineering and Biodesign Laboratory. At last I am very grateful for Dr. Ratnasingham Sooryakumar as my honor thesis oral defense committee member.

Table of Contents

List of Figures

Chapter 1: Introduction

1.1 DNA origami background

Origami refers to a Japanese art of folding and cutting flat paper into objects with desired shapes. DNA origami, invented by Rothemund in 2006,[1] is a novel approach to design and create nanostructures by self-assembly of a long single-stranded DNA (ssDNA), called scaffold DNA, with hundreds of short ssDNA, known as staple DNAs, to fold nanoscale objects with well-defined geometry[2] (Figure1.1). After decades of development, DNA origami can realize construction of lattice-based 2-D structures and bundle-based 3-D structures[3]. (Figure 1.2)

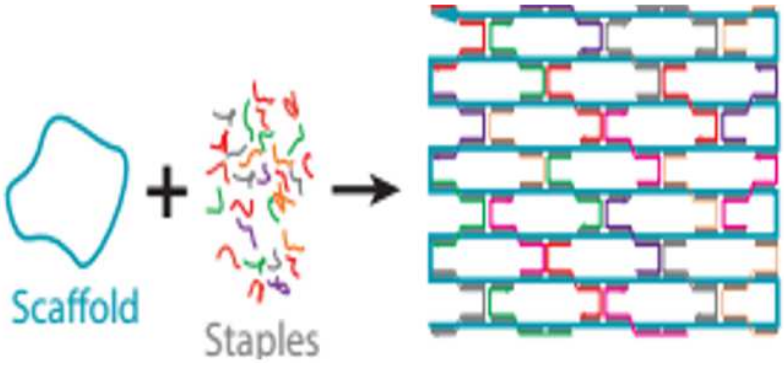

Figure 1.1: How scaffold and staples are binding to fold the origami (Modified from [2])

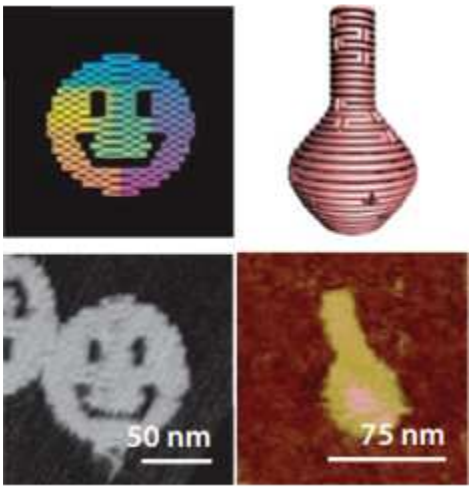

Figure 1.2: Lattice based 'smiling face' and bundle based 'drug deliver machine'(modified from [2])

Scaffold DNA origami typically utilizes scaffold DNA from the M13 bacteriophage genome DNA (7,249nt) or similar sequences 7560, 7704 and 8064 base[5]. The staple strands are typically synthesized by a commercial vendor (e.g. Integrated DNA Technologies or Eurofins Genomics) with length less than 60 bases. During self-assembly, staple strands will bind to the scaffold in a piecewise and sequence-specific manner to form the desired shape[4]. The folding is carried out in a slow annealing process that ranges in time from hours to days[5]. During the folding process, optimizing the assay condition such as magnesium or sodium concentration, folding temperature and staples to scaffold ratio is necessary to achieve yield high folding of nanostructures with well-defined geometry[5,6]. Typical yields can vary from ~10-90% with optimized folding conditions, depending on the complexity of the structure. Hence a purification is necessary to separate well-folded structures from mis-folded or aggregated structures and to remove the excess staple strands present in the folding reaction. Typically, purification method includes polyethylene glycol centrifugation and agarose gel electrophoresis[6,7]. Using the agarose gel electrophoresis can also give a quick check about whether the structures are folded by comparing the displacing distance between the scaffold used in the folding and the folded structure. After purification, transmission electron microscopy (TEM) will be used to image the nanostructures[6].

1.2 Dynamic and reconfigurable DNA origami

The ability to design nanostructures with precise complex geometries, combined with the ability to incorporate flexible single-stranded DNA domains that can facilitate motion, provides a foundation for building DNA-based nanomachines. Such nanomachines can sense and react to the environment, transfer motion, force, energy and information[3,10]. To fulfill these tasks, a dynamic DNA-based device requires integration of various components with precisely controlled relative motions. Analagous to macroscopic machines that consist of stiff components, called links, connected via joints that facilitate controlled relative motion, dynamic DNA origami mechanism can use stiff double-stranded DNA (dsDNA) as links and flexible ssDNA as joints.[8] Integration of these components enables design of different functional DNA nanodevices can make linear, rotational motion and complex motion combining the linear and rotational motion. For example, Figure 1.3 depicts a DNA revolute joint with rotational motion, a DNA slider with linear motion and a DNA crank slider that combines rotational and linear motion to achieve complex motion. (Figure 1.3 modified from [8])

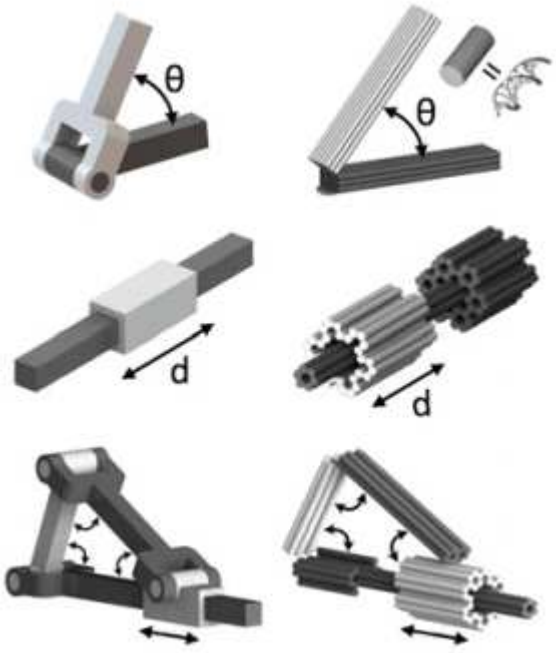

Figure 1.3: DNA revolute joint, DNA slider, and DNA crank slider (modified from [8])

In previous efforts, DNA origami has introduced to build reconfigurable quasi-fractal pattern in the method of 'fold-release-fold by multiple strand displacement and hybridization[9]. In Figure 1.4, it shows a continuous forward and reverse reconfiguration for a quasi-fractal pattern. It gives the potential to reconfigure a structure many times with adding strands in different sequency.

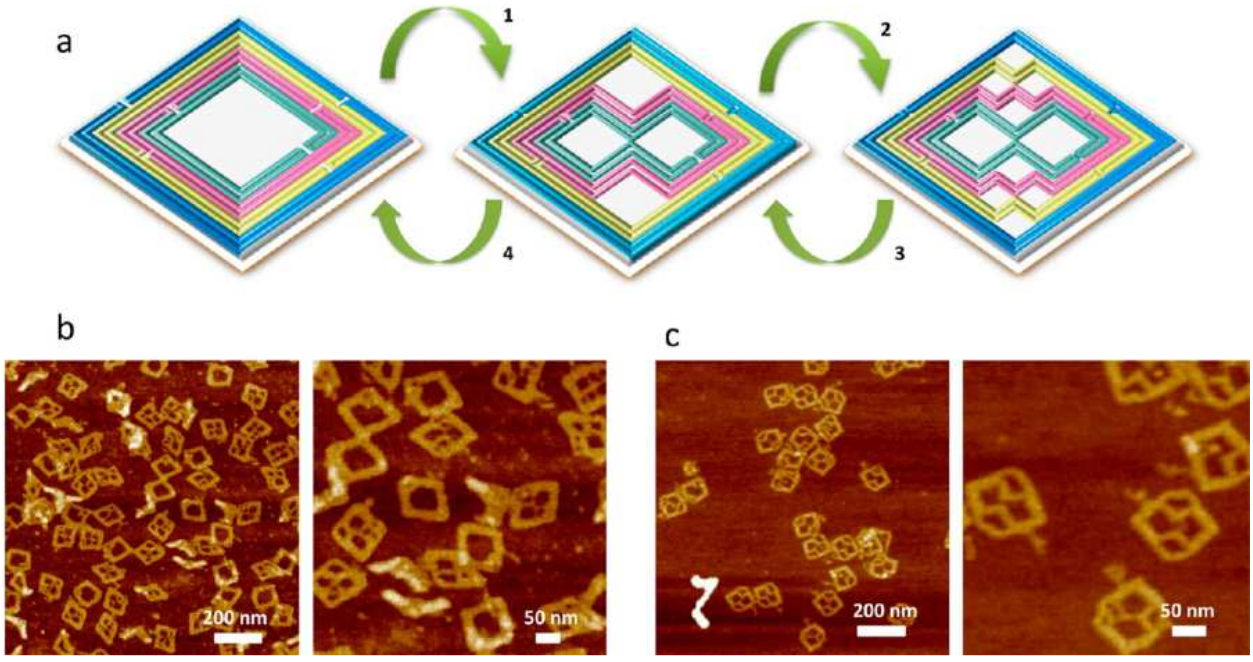

Figure 1.4: Continuous forward and reverse reconfiguration (modified from [9])

1.3 Actuation mechanisms

A rapid and reversible actuation mechanism is critical to controlled movement in robotic DNA nanodevices and assemblies. These actuation mechanisms can be broadly divided into three classes: molecular binding-based actuation, environmental cues-based actuation, and field-

induced actuation[10]. The most popular actuation approach is a molecular binding mechanism referred to as toehold mediated strand displacement (TMSD), which uses DNA strands that disrupt existing base-pairing interactions through competitive binding for actuation[14,11]. In Fig. 1.5 it shows how TMSD works to drive motion of a DNA walker along a track through sequential DNA binding and TMSD steps[13].

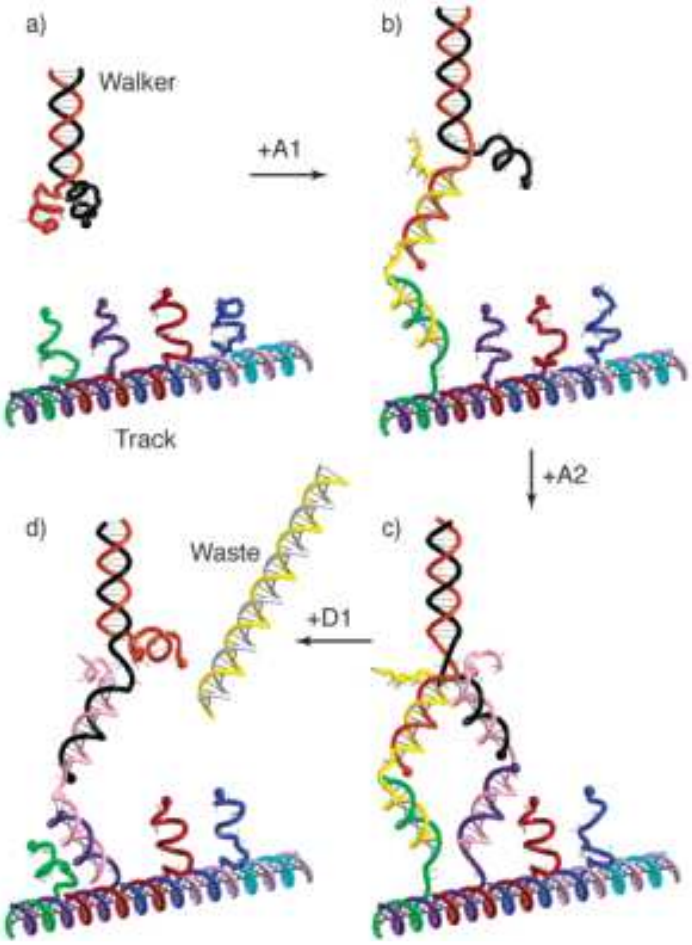

Figure 1.5: A synthetic DNA Walker for molecular Transport (modified from [13])

However, the response time for TMSD is on the scale of minutes to tens of minutes which is very slow for many robotic applications[11]. Environmental cues-based actuation uses

pH, ionic concentration, light, temperature and hydrophobicity to actuate DNA nanodevices[10]. Although these actuation mechanisms can have faster response times than TMSD, for many the timescale can still be minutes or greater. Furthermore, these methods only provide latching by stabilizing or releasing specific interactions as opposed to direct articulation of the structure for real-time control of DNA nanodevices. Thus, recent work has focused on new actuation methods for real-time articulation of DNA devices via electric and magnetic fields. Electric fields, for example, has been demonstrated to achieve sub-second response times[16]. However, electric field actuation has its own drawback that electric field will affect DNA-based elements, which are negatively charged, in the DNA assemblies which means controlling separate components is challenging[3]. Furthermore, objects must be tethered to avoid electrophoresis of the entire structure. Magnetic actuation, on the other hand, allows tunable application of various loading conditions to individual components[3]. For example, adding a super-paramagnetic bead to the end of the rotor system or the hinge system (figure 1.6) then actuated by external magnetic fields, providing real-time control on complex and continuous motion of nanostructures. Because of external magnetic fields is applied to all the samples, the magnetic manipulation platforms can be used as platforms for parallel actuation of many devices[12]

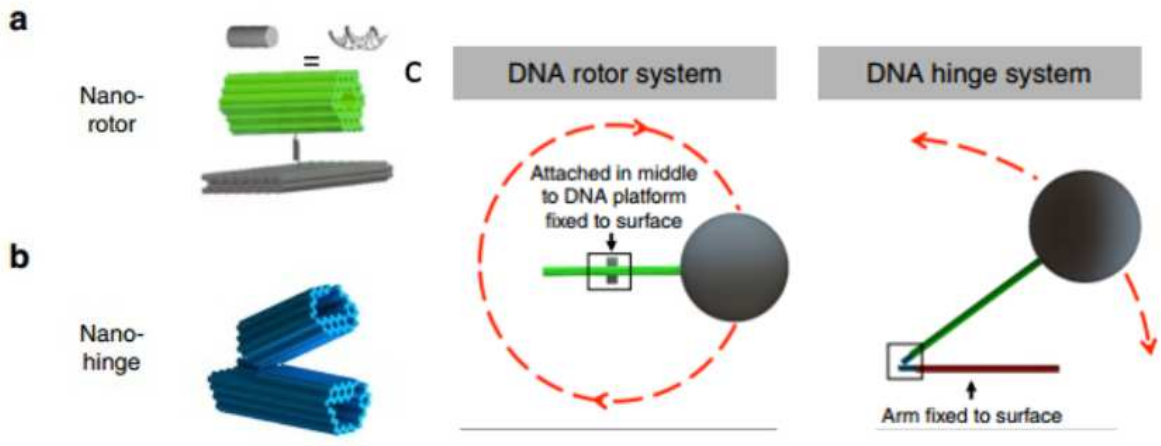

Figure 1.6: Magnetic actuated nano-rotor and nano-hinge (modified from [12])

There are two topics included in this thesis. The first topic is about reconfigurable 6-bar mechanism which is actuated by TMSD actuation mechanism to provide more complex reconfiguration in large assemblies (Chapter 2). The second topic is about optimizing assembly of micro-lever arms used in magnetic actuation (Chapter 3).

Chapter 2: Reconfigurable 6-Bar DNA origami

Currently, reconfiguration is limited to the single-device scale. In this work, we focused on a DNA origami structure capable of higher-order assembly into tubes with reconfigurable cross-sections in order to extend control over DNA nanostructure shape to the micron-assembly scale . I worked closely with graduate student Anjelica Kucinic. This project was part of her Master's thesis. I led the development and optimization the actuation methods to fold, purify, and reconfigure individual 6-bar reconfigurable devices into different cross sections to provide a framework for the higher order assembly reconfiguration.

2.1 Design and the reconfigurable 6-Bar DNA origami mechanism

The reconfigurable 6-bar mechanism consists of 6 bundles and each bundle is formed by 12 dsDNA helices arranged in a 3x4 square lattice cross section. (fig. 2.1)

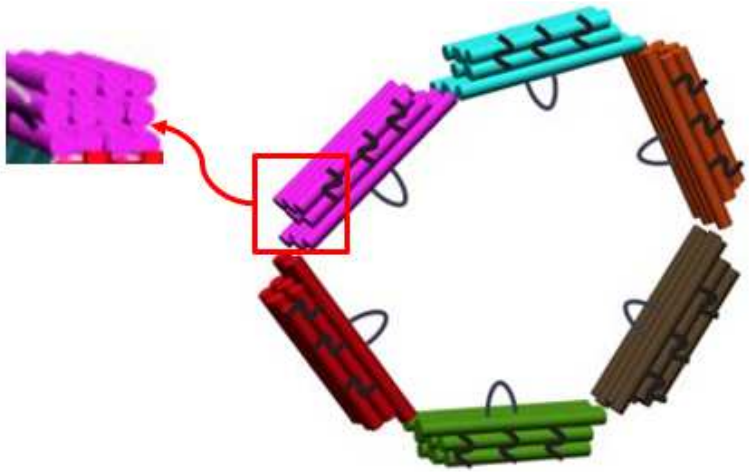

Figure 2.1: Reconfigurable 6-bar schematic

Between two bundles there are flexible ssDNA connections joining them together form a closed loop, but allowing flexible rotation between two neighboring bundles. Inside the 6-bar mechanisms, there is a 172nt scaffold loop attached on each bundle. These scaffold loops can be connected together through the addition of staple strands that bridge two scaffold loops together to form a stiff strut with controllable length. Pairing different scaffold loops together with particular length struts allows for configuring the 6-bar mechanism into a specific shape. There are five configurations for the 6-bar mechanism. The first configuration is the opened-loop (i.e. no strut) configuration which is flexible. The other four configurations require formation of struts where two scaffold loops are connected by staples (ssDNA) to form dsDNA struts to connect two neighboring bundles at a specific angle. Forming 4 different struts can thereby force the 6-bar mechanism into different shapes. Figure 2.2 shows how struts connect two scaffold loops. The struts can lock neighbor bundles into 60°, 90°, 120° and 180°, which can form rectangle, triangle, hexagon and flat closed configurations. The rectangle and triangle configuration contain two and three 180° trusses separately for staples to connect bundles adjacent to each truss into a colinear bundle. Fig 2.3, it shows the four configurations and the green parts represent the 180° trusses.

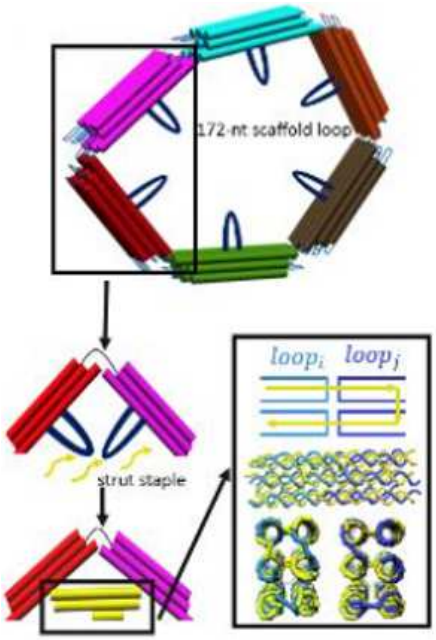

Figure 2.2: Struts formation (modified from [15])

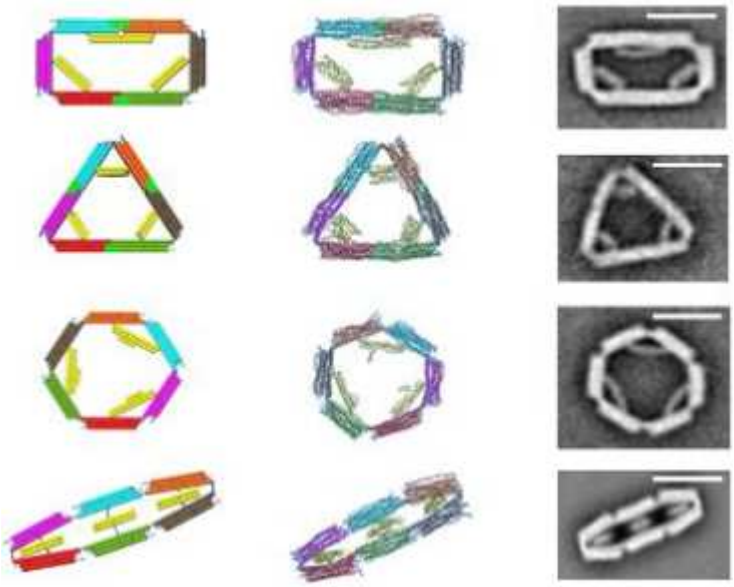

Figure 2.3: Four configurations for reconfigurable 6-bar mechanism (modified from [15])

2.2 Actuation method for reconfiguration

The actuation mechanisms used to form and disassemble struts are DNA strand binding and TMSD. The staple strands that comprise the struts all contain ssDNA toeholds. This allows for these staples to be removed through TMSD. When these strut staples are removed, the 6-bar mechanism will change to the free (i.e. no strut) configuration. In Fig 2.4, it shows the displace step where purple strands represent the rectangle displace staples and the yellow strands represent the staples binding the scaffold loops. After the displace step, excess replace staples will be added to deactivate the displace staples and the residual replace staples will reconstruct the struts and change the configuration as desired, which is called replace step. In figure 2.5 it shows the replace step where replacement staples for a particular configuration (e.g. flat closed) are added to reconstruct the dsDNA struts and the configuration changes from the free no strut configuration to the target configuration (e.g. flat closed).

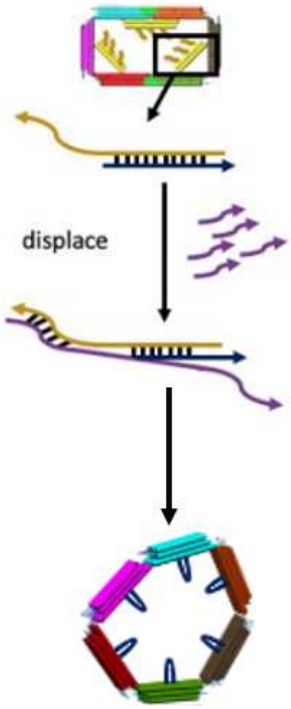

Figure 2.4: Displace Step from rectangle to open-struts configuration

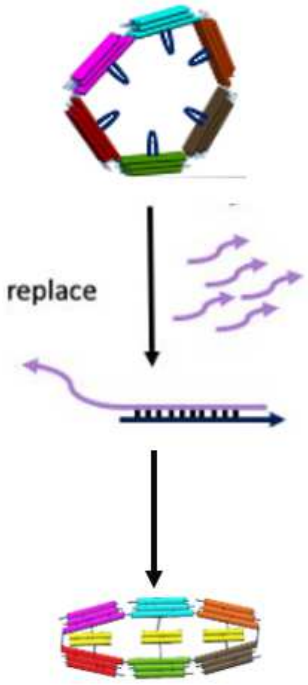

Figure 2.5: Replace step from open-struts configuration to flat-close configuration

2.3 Experiment method

The reconfiguration experiment is divided into 4 steps. The first step is folding, during this step reconfigurable 6-bar structures are folded into an initial configuration. This step required optimizing magnesium concentration for folding of each particular configuration. The second step is purification. We performed purification using centrifugal filter units following previously described protocols[17]. In this process, folded structures are added into centrifugal filters (e.g. Amicon filters) that contain a filter membrane with pores that allow staple strands to pass through but retain the larger folded DNA origami structures. The folding reactions are placed into the units and then centrifuged to get rid of excess staples. Pure, high concentration of folded structure can be obtained. The third step is a displacement step where 10x excess displace

staples relative to the structure concentration will be added. The last step is replace step where 10x excess replace staples relative to the displace strands' concentration will be added. Additionally, a small volume of Magnesium should be added to keep the salt concentration.

The folding reaction for all 6-bar mechanism configurations is consist of:

30nM 7249 base Scaffold

100nM staples (for corresponding configuration)

5mM Tris

5mM NaCl

1mM EDTA

$MgCl_2$ (optimized concentration for each configuration)

The magnesium concentration for each configuration is different so optimization in Mg^{2+} has been conducted. The results are shown in the result and discussion part.

After getting the optimized concentration of $MgCl_2$ for each configuration. Remake the folding reaction then put the fold reaction in annealing ramp from initial annealing temperature at 65°C to final preserving temperature 4°C at 1°C/30 min for 2 cycles. Next, purification with centrifugation with Amicon filters will be conducted at 10xG speed for 10 minutes to get rid of excess staples from the folding reaction. Then, measure the concentration for each folded structure and dilute them to 10nM for conducting displace step and replace step.

For the reconfiguration process, the displacement step was conducted firstly by adding 10-fold excess of displacement staples relative to the concentration of folded structure. Then the solution was placed into a thermal cycler for 2hrs incubation time at 37°C. Once structures are

displaced, I added 10x excess of replacement staples relative to the concentration displacement staples and added a small amount of high concentration $MgCl_2$ to increase the $MgCl_2$ concentration to 20mM. The solution was put into the thermal cycler in an annealing ramp from 45°C to 20°C at 2°C/hr for 2 cycles. The results of displacement and replacement were evaluated by gel electrophoresis and transmission electron microscopy. After displace step and replace step take out 5uL solution for transmission electron microscopy (TEM) preparation and imaging.

2.4 Result and discussion

2.4.1 Optimized Mg^{2+} concentration for each configuration

The results shown below are with agarose gel of $MgCl_2$ (mM) gradient after a 2.5 days fold for directly folding the 6-bar mechanisms into the various initial configurations.

Rectangle:

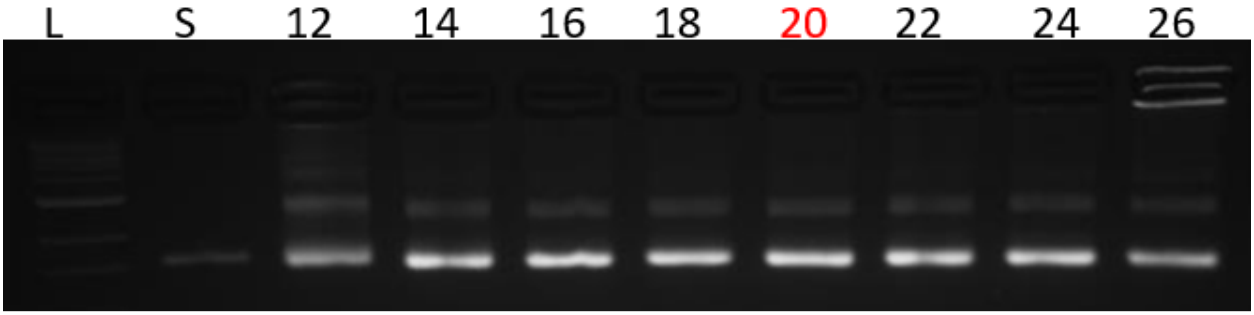

Figure 2.6: Agarose gel image with $MgCl_2$ (mM) screen for rectangle configuration

From the agarose gel, we observe that the rectangle folds well across the entire range of $MgCl_2$ conditions. We chose 20mM $MgCl_2$ for folding, which leads to a high yield of folded rectangle structures with no aggregation (aggregation is present in the well at 26 mM).

Triangle:

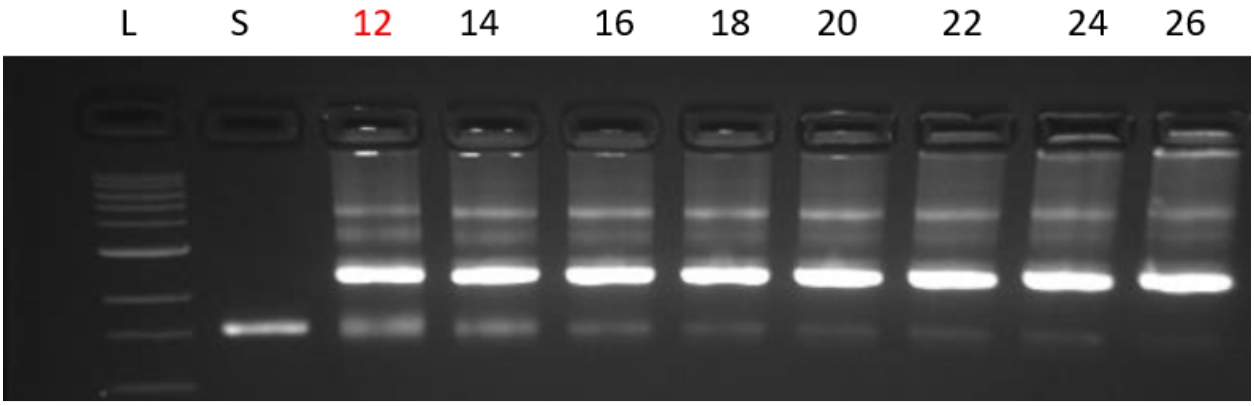

Figure 2.7: Agarose gel image with $MgCl_2$ (mM) screen for triangle configuration

From the agarose gel, we observed a weak fast running band that migrated similar to the scaffold and a strong slower running band. TEM imaging revealed the faster running band was the individual triangle, while the slower strong band was a dimerized triangle structure. We chose 12mM $MgCl_2$ as the best result, which led to the highest concentration of single triangle structures in the range we tested.

Hexagon:

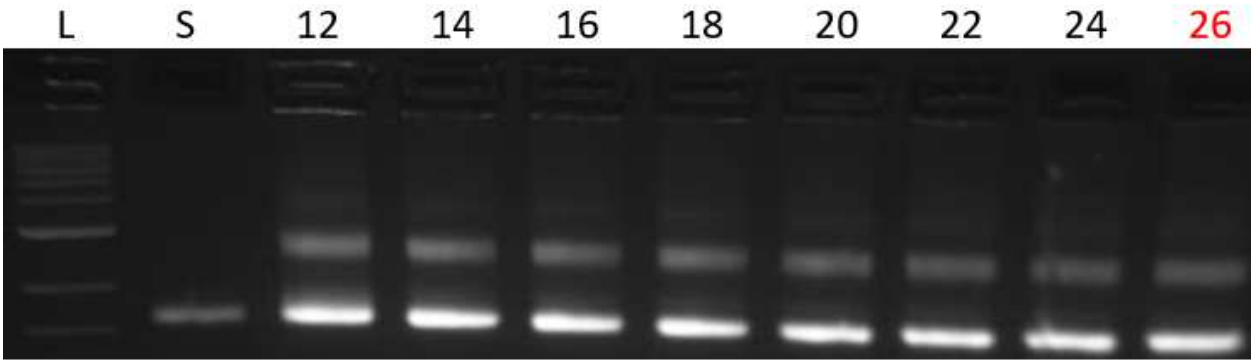

Figure 2.8: Agarose gel image with $MgCl_2$ (mM) screen for hexagon configuration

From the agarose gel, we observed that the hexagon structures folds well across the full range $MgCl_2$ concentrations we tested. However, it appears the higher concentration has less of a trailing smear and may run slightly faster. Hence, we chose 26mM $MgCl_2$ as the best result with for folding the hexagon structures.

Flat closed:

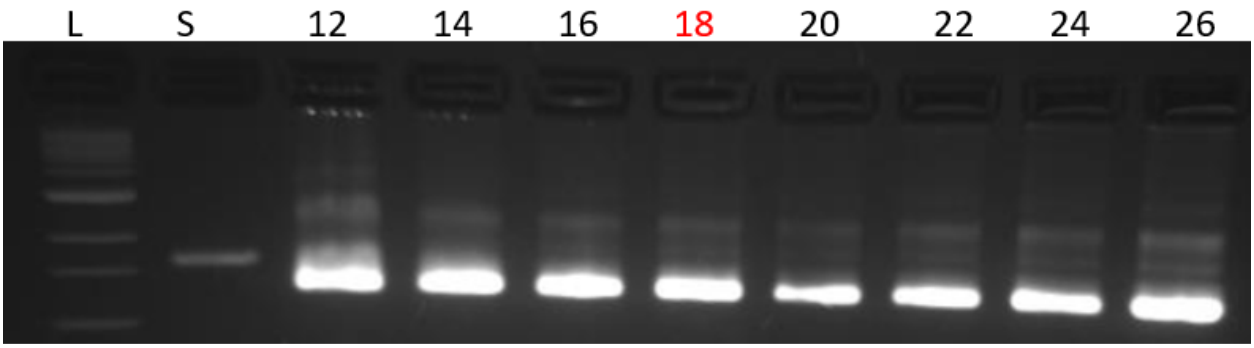

Figure 2.9 Agarose gel image with $MgCl_2$ (mM) screen for flat close configuration

From the agarose gel, we observed that the flat closed structures folds well across the full range $MgCl_2$ concentrations we tested. However, it appears the higher concentration has less of a trailing smear and may run slightly faster. Hence, we chose 18mM $MgCl_2$ as the best result with for folding the hexagon structures.

2.4.2 Reconfiguration efficiency and section preference

In figure 2.10, it shows the displacement result for rectangle configuration and hexagon figuration. From the TEM images, the amicon purified rectangle and triangle are displaced to the free configuration (i.e. no struts). The efficiency of the displacements is about 90% which shows high yield for the displacement step as evaluated by TEM image inspection. In figure 2.11, it shows the replacement result from open-strut configuration to flat-close and triangle. The efficiency for the replacement is about 70% which shows high yield for the replace step. The difference between displace and replace efficiency may come from the difference in salt concentration and cross section preference. From displace step to the open-struts configuration, the concentration of Mg^{2+} is at high state. But after adding displace staples and replace staples, the concentration of Mg^{2+} is half of the initial Mg^{2+} concentration. Even though a small volume of high concentration of $MgCl_2$ is added in the replace step it cannot reach to the initial state. In this low Mg^{2+} environment close-struts structures are difficult to keep the configuration so the replace efficiency is lower.

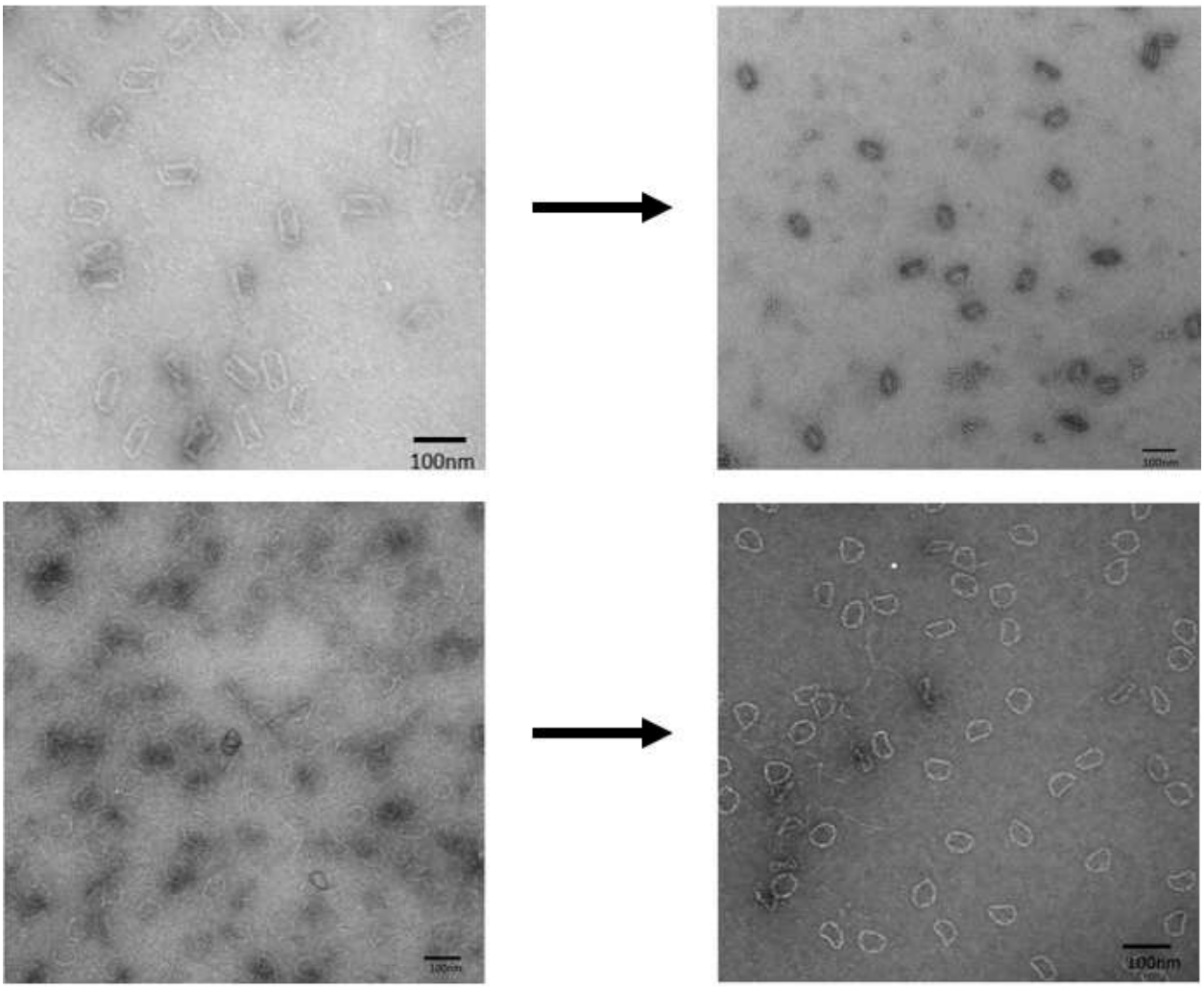

Figure 2.10: Displace step for rectangle and hexagon

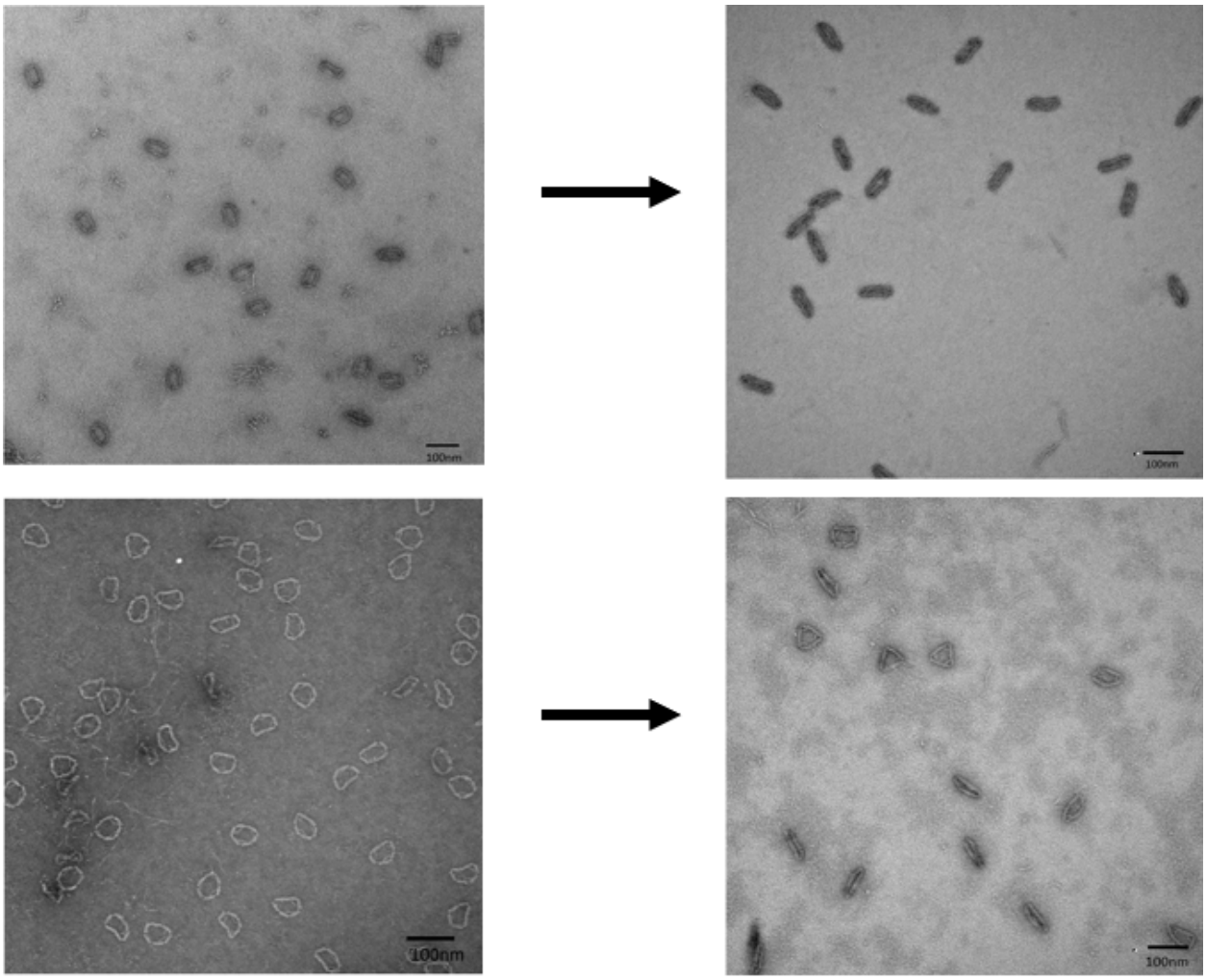

Figure 2.11: Replace step to flat-close and triangle

The difference in displace and replace efficiency may also come from the cross section preference. In figure 2.12 it is a agarose gel image for verification of the cross section preference where the initial configuration are still rectangle and hexagon configuration. But some modification has been made here. For rectangle reconfiguration, a control group where displace staples are not added during the displace step. Then both regular configuration group and control group will replace to flat-close configuration. For hexagon reconfiguration, one control groups is

added, as well. The first control group is without displace staples and after reconfiguration process it will replace to triangle and flat-close. The flow chart for the whole process is shown in figure 2.13. From the agarose gel, RRF and RWDF travel different distance in the gel which means the displace step for rectangle is necessary for rectangle changing to flat-close. HWDF and HRF, HWDT and HRT are both at the same distance which means displace step is not necessary for hexagon change to flat-close and triangle. Because toehold mediated strand displacement is used in the reconfiguration process where energy is input during the thermal actuation. It can be seen that hexagon has a lower energy barrier to get to the transition state, therefore a displacement step is not necessary to go to a final configuration of flat-closed and triangle. The displacement step is necessary for the rectangle to reach the final configuration of the flat-close configuration, as shown in the gel. Without displacement during the rectangle reconfiguration experiments, the final configuration is a transition state somewhere between the rectangle and flat-closed configurations.

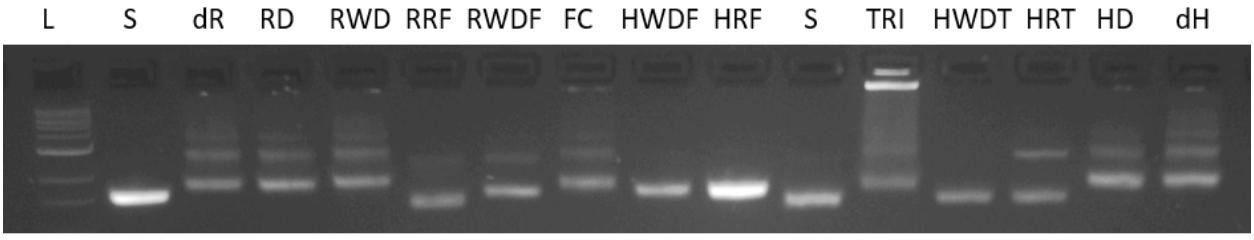

Figure 2.12: Agarose gel image for cross section preference

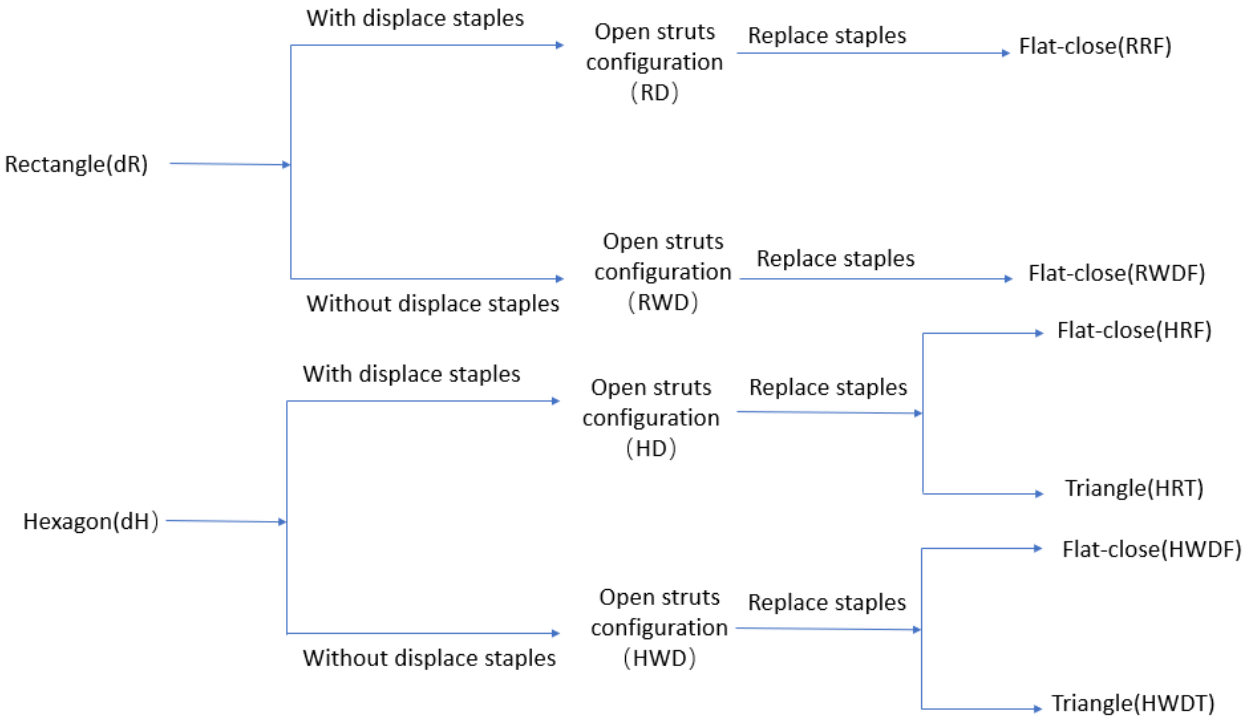

Figure 2.13: Flow chart for whole process

Chapter 3: Optimization for multiplexing magnetic actuated DNA origami lever

3.1 Introduction

Much like macroscopic robots, nanorobotic systems benefit from integration of many separate components and devices. Here this topic focuses on the actuation of one type of DNA structure, a microscopic lever arm previously presented in[12]. This microscopic lever arm has previously been used as an attachment on DNA nanostructures to control devices including a nano-hinge and a nano-rotor[12]. Similar devices have previously been used to measure the interactions between biomolecules and probe the stability of molecular complexes[10]. However, applying forces onto these DNA devices is typically challenging. Magnetic actuation provides a useful approach to implement forces under various loading conditions. Furthermore, with a multiplexing system force measurement for different nanodevices or repeated measurements for one nanodevice can be conducted simultaneously so that the measurement efficiency can be greatly increased. The microscopic lever arm is assembled by the nano-bricks, which we also refer to as monomers. A monomer consists of 56 dsDNA helices bundled together into a compact cross-section (Figiure 3.1, left). These monomers can be polymerized in 1-D direction to form a microscopic lever arm (figure 3.1, right).

Motivated by hinge actuation where separate lever arms attach to two separate arms of the hinge. There is another version of monomer called monomer 2. Monomer 2 has the same components and shape as monomer 1 except there are 5 overhangs attached at the bottom which can bind with the biotin labeled strands on an operated platform. Then one arm of the hinge can be anchored to the surface. (figure 3.2)

Figure 3.1: monomer 1 and microscopic lever arm 1 (modified from [12])

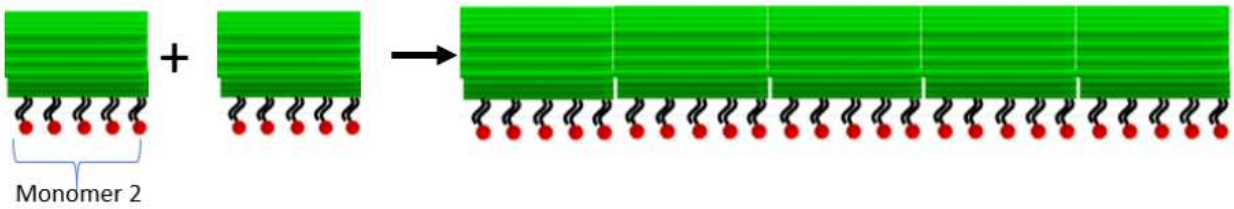

Figure 3.2: monomer 2 and microscopic lever arm 2 (modified from [12])

3.2 Research goal

The overall goal of this work is to build a foundation for nanorobotics especially in measurements in the stability of biomolecular and molecular complexes. To achieve this goal we have planned the following specific objectives:

Objective 1: We will build a multiplexed magnetic actuation system as the platform for parallel control of multiple nanodevices. To achieve this goal, the yield of actuated nanodevices should be increased so that the number of constructs can increase from ~1 – 2 to $\geqslant$ 10 in a 80 x 80 µm field of view (figure 3.3)

Objective 2: To have practical application in the measurements in the stability of biomolecular and molecular complexes, the length of the microscopic lever arm should be increases from <1

µm to 1-2 µm.

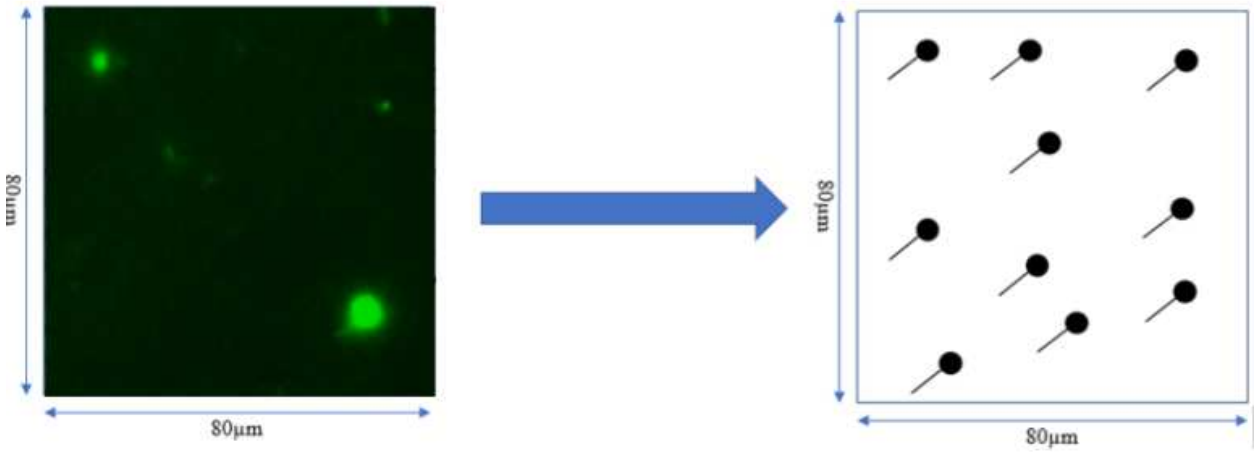

Figure 3.3: Increase the yield of the microscopic lever arms from ~1-2 to ⩾ 10 in a 80 x 80 µm field of view (modified from [12])

3.3 Experiment methodology

The experiment was divided into three parts. The first part is monomer optimization. In this part magnesium concentration and staple to scaffold ratio in the folding reaction will be optimized. The second part is polymer yield optimization. In this part, we will optimize the polymerization (i.e. maximize length of polymers while minimizing aggregation) as a function of monomer concentration and the addition of detergent to reduce the aggregation. The third part is additional polymer length optimization. In this part, additional monomer will be added after 1st round of polymerization to lengthen the polymers through a second round of polymerization.

The folding reaction for the monomer is consisted of

30nM 7249 base Scaffold

staples (to be optimized)

5mM Tris

5mM NaCl

1mM EDTA

$MgCl_2$ (to be optimized)

This folding reaction is subjected to an annealing ramp with initial temperature at 65°C for 15 min then cooled from 65 °C–20°C at 5°C /h and preserved at 4°C .For the monomer magnesium concentration optimization, a $MgCl_2$ screen of 12mM, 14mM, 16mM, 18mM, 20mM, 22mM, 22mM, 24mM, 26mM will be conducted in the agarose gel, please see the detailed protocol in the reference. With the optimized Mg^{2+} concentration, the staple to scaffold ratio at 2x, 2.5x, 3x, 3.33x will be chosen from the result of agarose gel. Once monomer folding is optimized, we will purify them via centrifugal filtration using amicon filters at 10G speed for 10 minutes for 3 times to get rid of excess staples. With purified monomers, measure the concentration and then dilute them to 30nm for polymerization optimization.

During the polymerization yield optimization, we first tested the use of detergent to inhibit aggregation. The detergent reaction is consisted of 10nm purified monomer, 5x excess polymerization staples relative to the monomer concentration, 10mM $MgCl_2$. Similar reactions with the addition of 0.2% NP40 has also been made. Then put the polymerization reaction in the thermal cycler and anneal from 45°C to 4°C at 1.5°C/h for 2 cycles, based on previously used annealing protocols for polymerization[13]. After the detergent test, we remade the polymerization

reaction with monomer concentration at 5nm, 10nm and 20nm then put the polymerization reaction in the thermal cycler and anneal from 45°C to 4°C at 1.5°C/h for 2 cycles.

During the polymer length optimization, the first round of polymerization was conducted based on the result of detergent and monomer concentration above.

3.4 Result and discussion

3.4.1 Monomer optimization

In fig 3.4, it is the agarose gel image of magnesium concentration optimization for monomer 1 and monomer 2. From the gel, 20mM $MgCl_2$ is optimized for monomer 1and 26mM $MgCl_2$ is optimized for monomer 2.

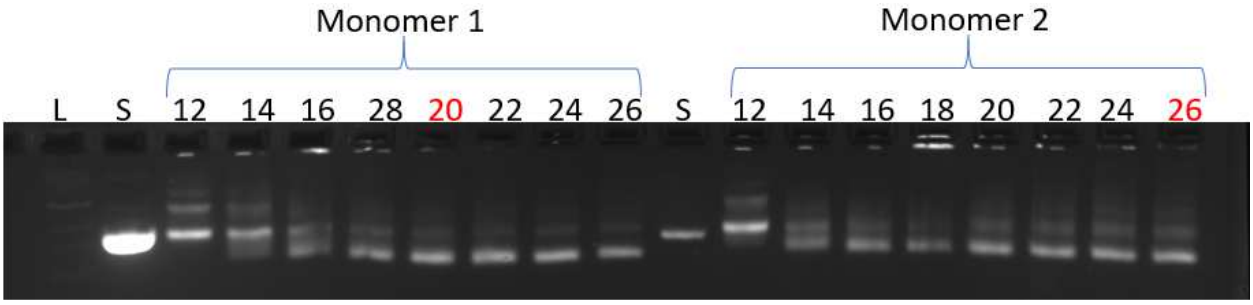

Figure 3.4: Agarose gel image for magnesium concentration optimization for monomer 1 and monomer 2

In fig 3.5 it shows the result for the optimization of staple to scaffold ratio. From the agarose gel, staple to scaffold ratio at 3.33x is optimized for monomer 1 and 2.5x is optimized for monomer 2.

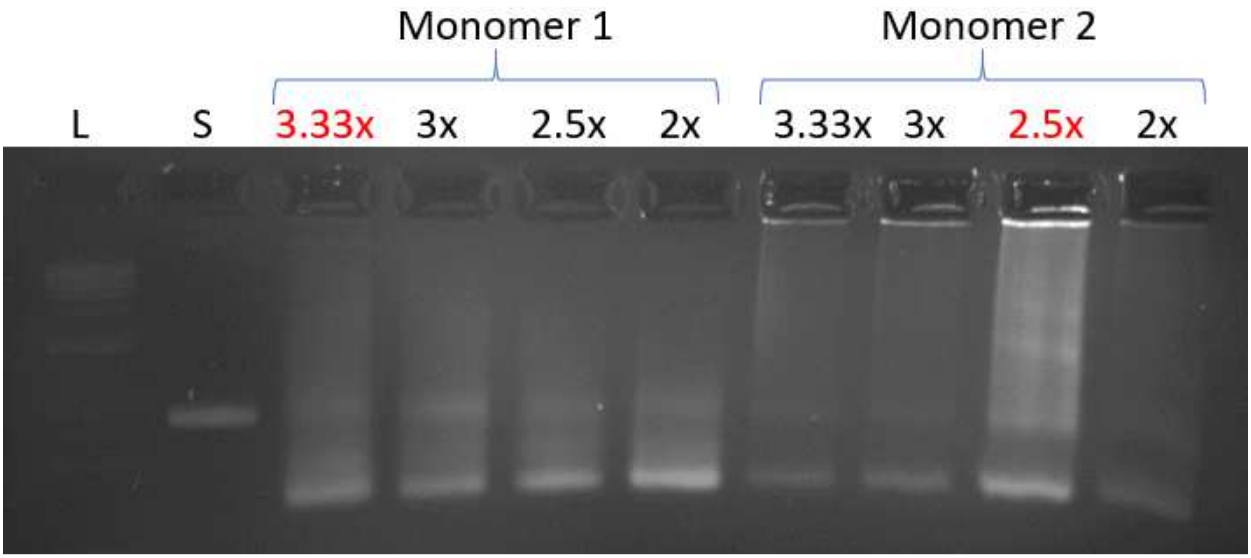

Figure 3.5: Staple to scaffold ratio optimization for monomer 1 and monomer 2

3.4.2 Polymerization yield optimization

Figure 3.6 shows the result for the detergent test. From the agarose gel, the polymer 1 with detergent and polymer 1 without detergent are both stuck in the gel wells which represents the polymerization works. From TEM image, the without detergent polymer 1 has much more aggregation than the with detergent polymer 1. So detergent is necessary to reduce the polymer aggregation.

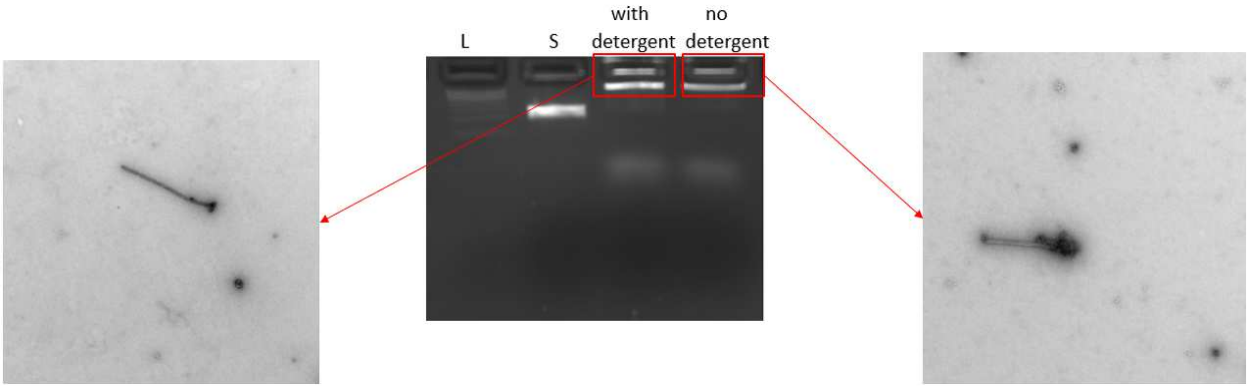

Figure 3.6: Agarose gel image for detergent test

In figure 3.7, it shows the result for the initial monomer concentration optimization in the polymerization reaction. From the agarose gel, 20nM initial monomer concentration gives the highest concentration and from the TEM image it shows the yield of the polymer 1 is still low but the length for the polymer reaches to 1µm.

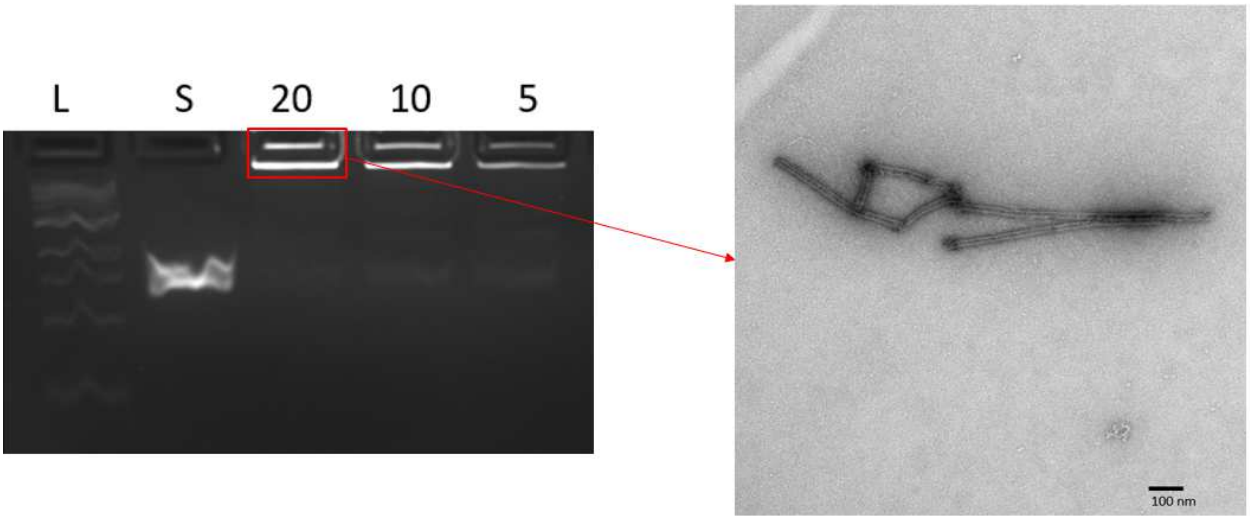

Figure 3.7: Initial monomer concentration optimization for polymerization

Due to the shut down during the COVID19 pandemic, there was not enough time for completing the polymer length optimization. In future research, a polymer length optimization will be conducted which consists of 2 rounds of polymerization and during the second round of polymerization additional monomers will be added to increase the length of polymers.

Chapter 4 Conclusion

The design for the reconfigurable 6-bar mechanism is feasible and the yield for the folding process is very high. During the reconfiguration process, the efficiency for the displace step can reach to 90% and the efficiency for replace step reaches to 70%. From the difference between the efficiency and the agarose gel image, rectangle does need the displace step to change the configuration to flat-closed but hexagon can change to the flat-close configuration without the displace step. We can conclude that hexagon configuration has more free energy than the transition state than the rectangle configuration. Further study will focus on the cross section preference and stiffness for each configuration.

The optimized assay condition for microscopic lever arm is with 20mM $MgCl_2$, 3.33x staple to scaffold ratio for monomer 1 and 26mM $MgCl_2$, 2.5x staple to scaffold ratio for monomer 2 in the folding reaction. And for polymerization, 0.2% NP40 is necessary for reducing the polymer aggregation and 20nm concentration is the optimized initial monomer concentration for polymerization. From the TEM image, it can be concluded that the yield of the polymer is still low but the length for the polymer reaches to 1µm which means the goal is initially achieved for the polymer length optimization.

This work realized and optimized reconfiguration for large DNA origami structures which is critical for building complex DNA origami machines with high order of freedom. Moreover, it provides base for building an multiplexing magnetic actuation platform for further biomolecular research such as force measurement.

Reference

[1] Rothemund, P. Folding DNA to create nanoscale shapes and patterns. Nature 440, 297–302 (2006). https://doi.org/10.1038/nature04586

[2] Ke, Yonggang et al. "Structural DNA Nanotechnology: Artificial Nanostructures for Biomedical Research." Annual review of biomedical engineering 20 (2018): 375-401.

[3] Dey, S., Fan, C., Gothelf, K.V. et al. DNA origami. Nat Rev Methods Primers 1, 13 (2021). https://doi.org/10.1038/s43586-020-00009-8

[4] Jean-Michel Arbona , Jean-Pierre Aimé & Juan Elezgaray (2012) Folding of DNA origamis, Frontiers in Life Science, 6:1-2, 11-18, DOI: 10.1080/21553769.2013.768556 https://doi.org/10.1080/21553769.2013.768556

[5] Douglas, S., Dietz, H., Liedl, T. et al. Self-assembly of DNA into nanoscale three-dimensional shapes. Nature 459, 414–418 (2009). https://doi.org/10.1038/nature08016

[6] Castro, C., Kilchherr, F., Kim, DN. et al. A primer to scaffolded DNA origami. Nat Methods 8, 221–229 (2011). https://doi.org/10.1038/nmeth.1570

[7] Stahl, E., Martin, T.G., Praetorius, F. and Dietz, H. (2014), Facile and Scalable Preparation of Pure and Dense DNA Origami Solutions. Angew. Chem. Int. Ed., 53: 12735-12740. https://doi.org/10.1002/anie.201405991

[8] Alexander E. Marras, Lifeng Zhou, Hai-Jun Su, Carlos E. Castro, Proceedings of the National Academy of Sciences Jan 2015, 112 (3) 713-718; DOI: 10.1073/pnas.1408869112

[9] Fei Zhang, Jeanette Nangreave, Yan Liu, and Hao Yan, Reconfigurable DNA Origami to Generate Quasifractal Patterns. Nano Letters 2012 12 (6), 3290-3295.DOI: 10.1021/nl301399z

[10] DeLuca, Marcello & Shi, Ze & Castro, Carlos & Arya, Gaurav. (2019). Dynamic DNA Nanotechnology: Toward Functional Nanoscale Devices. Nanoscale Horizons. 10.1039/C9NH00529C.

[11] Zhang, D., Seelig, G. Dynamic DNA nanotechnology using strand-displacement reactions. Nature Chem 3, 103–113 (2011). https://doi.org/10.1038/nchem.957

[12] Lauback, S., Mattioli, K.R., Marras, A.E. et al. Real-time magnetic actuation of DNA nanodevices via modular integration with stiff micro-levers. Nat Commun 9, 1446 (2018). https://doi.org/10.1038/s41467-018-03601-5

[13] Shin, Jong-shik & Pierce, Niles. (2004). A Synthetic DNA Walker for Molecular Transport. Journal of the American Chemical Society. 126.

[14] Yurke, B., Turberfield, A., Mills, A. et al. A DNA-fuelled molecular machine made of DNA. Nature ***406,*** *605–608 (2000). https://doi.org/10.1038/35020524*

[15] Anjelica Kucinic, Reconfiguration, actuation, and higher order complexity of dynamic DNA origami assemblies, 2020.

[16] Kopperger, E., List, J., Madhira, S., et al. A self-assembled nanoscale robotic arm controlled by electric fields. Science Vol. 359, Issue 6373, pp. 296-301 (2018) https:// doi.org/10.1126/science.aao4284

[17] Wagenbauer, Klaus & Engelhardt, Floris & Stahl, Evi & Hechtl, Vera & Stömmer, Pierre & Seebacher, Fabian & Meregalli, Letizia & Ketterer, Philip & Gerling, Thomas & Dietz, Hendrik. (2017). How we make DNA origami. Chembiochem: a European journal of chemical biology. 18. 10.1002/cbic.201700377.